Functionalized Two-dimensional Nanoporous Graphene (NPG) as Efficient Global Anode Materials for Li, Na, K, Mg, and Ca Ion Batteries

Tanveer Hussain[1,*], Emilia Olsson,[2] Khidhir Alhameedi[1], Qiong Cai[2,*] and Amir Karton[1,*]

[1]School of Molecular Science, The University of Western Australia, Perth, WA 6009, Australia
[2]Department of Chemical and Process Engineering, University of Surrey, Guildford, GU2 7XH, United Kingdom

*Corresponding authors: T. Hussain (tanveer.hussain@uwa.edu.au); Q. Cai (q.cai@surrey.ac.uk); A. Karton (amir.karton@uwa.edu.au)

Abstract

Two-dimensional nanoporous graphene (NPG) with uniformly distributed nanopores has been synthesized recently and shown remarkable electronic, mechanical, thermal, and optical properties with potential applications in several fields [Science 360, 199 (2018)]. Here, we explore the potential application of NPG as an anode material for Li, Na, K, Mg and Ca ion batteries. We use density functional theory calculations to study structural properties, defect formation energies, metal binding energies, charge analysis, and electronic structures of NPG monolayers. Pristine NPG can bind effectively K^+ cations, but cannot bind the other metal cations sufficiently strongly, which is a prerequisite of an efficient anode material. However, upon substitution with oxygen-rich functional groups (e.g., O, OH, COOH) and doping with heteroatoms (B, N, P, S), the metal binding ability of NPG is significantly enhanced. Of the considered systems, S-doped NPG (S-NPG) binds the metal cations most strongly with binding energies of -3.87 (Li), -3.28 (Na), -3.37 (K), -3.68 (Mg), and -4.97 (Ca) eV, followed by P-NPG, O-NPG, B-NPG, and N-NPG. Of the substituted NPG systems, O substituted NPG exhibits the strongest metal binding with binding energies of -3.30 (Li), -2.62 (Na), -2.89 (K), -1.67 (Mg) and -3.40 eV (Ca). Bader charge analysis and Roby-Gould bond indices show that a significant amount of charge is transferred from the metal cations to the functionalized NPG monolayers. Electronic properties were studied by density of states plots and all the systems were found to be metallic upon the introduction of metal cations. These results suggest that functionalized NPG could be used as a global anode material for Li, Na, K, Mg, and Ca ion batteries.

Keywords: Density functional theory, 2D monolayers, Metal Ion batteries, Nanoporous Graphene

Cite as:
T. Hussain, E. Olsson, K. Alhameedi, Q. Cai, A. Karton. *J. Phys. Chem. C* 124, 9734–9745 (2020). https://dx.doi.org/10.1021/acs.jpcc.0c01216

1. Introduction

Soaring energy demands caused by population increase and growing urbanization has led to unprecedented stress on conventional energy sources to maintain demand-supply chains. This situation coupled with limited reserves of current fossil fuel-based energy sources and their devastating effects on the environment has resulted in an urgent need for cleaner, efficient, renewable, and sustainable alternative energy solutions. **[1]** Hydropower, solar, geothermal and wind are a few of the available clean energy options, which are in need of proficient energy storage solutions. **[1]** Metal-ion batteries are considered one of the most viable technologies for the efficient storage of clean energy. **[2-4]** Lithium ion batteries (LIBs) are the front-runners among the metal-ion batteries due to the well-established technology, long-term cyclic stability, portability, and diverse range of applications from cellphones to electric automobiles. **[5-7]** However, despite their high energy density, availability of electrode materials, and ease of operation, limited lithium reserves coupled with high costs limit the application of LIBs in the longer run, especially for large-scale energy storage. **[8]** Thus, it is of interest to develop alternative and complimentary battery technologies, which would use sustainable resources and are cost effective.

Alkali metals such as Na and K are an obvious alternative for Li since they are abundant and widely available, which makes Na ion batteries (NIBs) and K ion batteries (KIBs) more cost effective compared to LIBs. **[8, 9]** Furthermore, it has been shown that the larger Na and K atoms exhibit similar behavior to that of Li in battery applications. **[10, 11]** Recently, divalent metal-ion batteries such as Mg ion batteries (MIBs) and Ca ion batteries (CIBs) have attracted considerable interest due to their ability of donating two valence electrons, and consequently doubling the overall hypothetical storage capacities. **[12]** Several other salient features like non-toxicity, abundance in the earth's crust, and cost effectiveness make this class of batteries a promising alternative to LIBs. **[13-15]** Although other multivalent cations such as Zn^{2+}, Ni^{2+} and Al^{3+} have also been considered as potential alternatives to the monovalent batteries, their drawbacks including large volume expansion, slow kinetics, and low voltages make these cations less efficient. **[12-18]** For all the available metal-ion batteries, challenges remain in designing efficient electrode materials. Specifically, the performance of metal-ion batteries could be hindered by the discharge cycle, and the battery lifetime in the absence of efficient anode materials. **[19, 20]** Thus, designing anode materials with high storage capacities, and capabilities of solving the challenges including irreversible capacity, power density, and short lifetime are keys for the transition towards more efficient metal-ion batteries.

Graphite is the commonly used anode material for LIBs where it works exceptionally well. **[3]** However, the weak binding interactions with the metal cations and smaller interlayer spacing restricts the application of graphite as anode materials for other metal-ion batteries including NIBs, KIBs, MIBs and CIBs. **[3, 11]** This has motivated researchers to look for efficient alternative anode materials that are capable of binding metal cations (Li^+, Na^+, K^+, Mg^{2+}, and Ca^{2+}) better than graphite. Carbonaceous nanostructures (CNs) in different morphologies are one of the most studied classes of materials due to their fascinating properties and widespread applications in various fields such as optoelectronics, spintronics, energy harvesting. **[21-24]** Two-dimensional (2D) CNs in particular have attracted significant attention due to their unique properties such as large surface to volume ratio, excellent thermal/dynamic stabilities, and robust diffusion of cations. **[25-27]** Various 2D materials have been considered as anode materials for MIBs, including modified graphene, **[28, 29, 48]** graphdiyne (GDY), **[19,31]** boron-graphdiyne (BGDY), **[30]** graphenylene, **[32]** biphenylene, **[33]** and carbon nitrides (C_3N_4 and C_6N_8). **[34,35]**

Nanoporous graphene (NPG) systems with different pore sizes have been synthesized and studied for various applications including optoelectronics, energy harvesting, and gas sensing. **[36-39]** Recently, a novel 2D NPG, consisting of ordered graphene nanoribbons, has been synthesized using a bottom-up approach. **[40]** This 2D NPG monolayer has uniformly distributed pores of 1 nm. This unique structure makes it a potential candidate for energy conversion and storage applications. A recent study used density functional theory (DFT) and classical molecular dynamics (MD) simulations to show that 2D NPG with uniform 1 nm pores is a semi-conductor, with interesting mechanical, thermal, and optical properties. **[41]** As far as we know, the potential application of this 2D NPG in energy storage as battery electrodes has not been investigated. Here, we explore the potential application of this material as an anode for LIBs, NIBs, KIBs, MIBs, and CIBs. We have employed dispersion-corrected DFT calculations to investigate the structural and electronic properties of pristine and functionalized NPG monolayers. The storage of single and divalent metals (Li, Na, K, Mg, and Ca) on the pristine and functionalized NPG are investigated in order to understand the suitability of these materials for applications in LIBs, NIBs, KIBs, MIBs, and CIBs.

2. Computational details

Spin-polarized first principle calculations based on DFT were performed using the Vienna *ab initio* Simulation Package (VASP). **[42, 43]** The generalized gradient approximation (GGA) with the Perdew-Burke-Ernzerhof (PBE) exchange-correlation functional was used. **[44]** The electron-ion interactions were treated with the projector-augmented wave (PAW) methods with a cut off energy of 500 eV for the plane-wave basis set. **[45]** It is well known that GGA methods tend to underestimate the binding energies thus the empirical van der Waals correction of Grimme (DFT-D3) was included. **[46]** We note that the same method was previously used by Mortazavi *et al.* to study the structural and electronic properties of NPG materials. **[37]** As per this previous study, all calculations employed a unit cell of 100 atoms (C = 80, H = 20) periodic along the X and Y-directions with a vacuum space of 15 Å along the Z-direction to avoid the possible vertical interactions between repeating layers. The Brillouin zone (BZ) was sampled by using the Monkhorst–Pack scheme with a mesh size of 2×4×1. **[47]** Convergence criteria for the total energies and forces were set at 10^{-6} eV and 0.01 eV/Å, respectively.

This work aims to understand and improve the binding energies of metal adatoms Li, Na, K, Mg and Ca with pristine and defected NPG. Metal binding energies (E_b) are calculated via:

$$E_b = E_{M@NPG} - E_{NPG} - E_M \qquad (1)$$

Here, $E_{M@NPG}$, E_{NPG}, and E_M represent the total energies of NPG with metal adatom, bare NPG and metal atom, respectively. It is important to mention that the total energy of the metal atoms was considered in its isolated form by placing it in a large box of dimensions 15Å◘15Å◘15 Å. Charge transfer mechanism between NPG and metal adatoms was studied using Bader charge analysis. **[48]** We note that in the geometry optimizations of the metals on the NPG and functionalized NPG (FNPG) we have started the optimizations from a number of M•••NPG and M•••FNPG distances to make sure that the lowest energy structure is obtained.

3. Result and discussion

3.1 Pristine NPG monolayer

Before studying the metal binding to NPG, we briefly describe the structural properties of the NPG monolayer. The optimized NPG monolayer has three different C-C bond lengths ranging between 1.38-1.43 Å, whereas all C-H bonds are found to have bond lengths of 1.09 Å, as shown in Figure S1 (Supplementary Information). Importantly, all C and H atoms are coplanar as shown in Figure 1 (b). The lattice vectors (a = 32.383 and b = 8.583 Å) are within 0.05 Å from those calculated with the PBE functional (without a dispersion correction). **[41]** The electronic properties of pristine NPG are studied by means of total and partial density of states (TDOS and PDOS, respectively) plots as shown in Figure 1 (c). Semiconducting behavior with a band gap (E_g) value of 0.63 eV is evident from the two DOS plots. Both the valence and conduction bands are dominated by the p orbitals of both types of C atoms (either bonded with C or H). We note that as expected our E_g value represents an underestimation, e.g., an E_g value of 0.88 eV is obtained with the more accurate HSE06 hybrid GGA functional. **[41]**

To consider the suitability of NPG as an anode material for metal-ion batteries, binding energy (E_b) values of metals with the NPG materials are calculated. The metal cations Li, Na, K, Mg, Ca should have E_b higher than their corresponding cohesive energies (E_c) to ensure efficient binding without clustering. In total, 17 different available metal binding sites, as shown in Figure 1 (a) are considered to identify the most stable metal adsorption sites. The lowest energy configurations yielded E_b values of -1.52, -0.70, -1.42, -0.35 and -1.08 eV for Li, Na, K, Mg and Ca, respectively (Table S1 in the Supporting Information). The corresponding E_c values of Li, Na, K, Mg and Ca are -1.63, -1.11, -0.93, -1.51 and -1.84 eV, respectively. **[49-51]** Thus, only for K we obtain $E_b > E_c$ (by 0.49 eV), which prevents the application of pristine NPG as an anode material for the other metals. One strategy for improving the metal adsorption properties of NPG is by (i) oxidizing the sheet (i.e., substitution with oxygen-containing functional groups), and (ii) doping with heteroatoms (N, P, S, and B).

3.2 Defects in NPG monolayers

Generally, CNs are associated with a number of defects, which can have a significant influence on their properties. Here, we investigate the effect of two types of defects on the structural, electronic and metal storage properties of NPG monolayers. In particular, we

consider (i) functionalized NPG in which hydrogens are substituted with a selection of three oxygen-containing functional groups: carbonyl oxygen (=O), hydroxyl (–OH), and carboxyl (–COOH) groups, and (ii) doped NPG in which a carbon atom is replaced with an heteroatom (B, N, P, or S).

We begin by considering the formation energies (E_f) associated with the considered defects, which are calculated according to the following equation: **[52]**

$$E_f = E_{FNPG} - E_{NPG} - \mu_i + \mu_H + \mu_C \quad (2)$$

Here, E_{FNPG} and E_{NPG} are the total energies of the functionalized and pristine NPG monolayers, respectively; μ_i is the chemical potential of the substituents (O, OH, COOH) or dopants (B, N, P, S), μ_H and μ_C are the chemical potentials of the substituted C and H atoms. Following Eq. (2), a small defect formation energy E_f indicates the ease of creating a specific defect and energetically stable configuration. It is worth noting that E_f can be directly coupled to a defect concentration under equilibrium conditions, with lower E_f indicating higher defect concentrations. The calculated E_f values for the defects and substitutions are summarized in Table 1.

Table 1. Defect formation energies (E_f, in eV) for the functionalized NPGs at different inequivalent sites as shown in Figures S2–S8 of the Supporting Information.

	Defect	Site I	Site II	Site III
Substituted NPG	=O	-2.22	-2.24	-2.20
	-OH	-0.51	-0.56	-0.50
	-COOH	1.28	1.13	0.74
Doped NPG	B	0.41	0.41	0.75
	N	-0.52	-0.55	0.00
	P	2.37	2.36	2.12
	S	3.77	3.76	3.98

Inspection of the formation energies in Table 1 indicates that substitution of a hydrogen with an oxygen atom is highly exothermic with E_f values ≤ -2.2 eV depending on the substitution site (Figure S2, Supporting Information), whereas substitution with a

hydroxyl group results in smaller E_f values ≤ -0.5 eV. Of the considered doped NPGs, only nitrogen doping is thermoneutral or exothermic with E_f values ranging between 0.0 and -0.55 eV. Doping with B is associated with small positive E_f values of up to 0.75 eV. Doping with either P or S atoms is energetically less favourable as indicated from significantly larger formation energies ranging between 2.12 – 3.98 eV. We note that similarly high formation energies are observed for P and S doping in graphene. **[53-56]** Nevertheless, the E_f values of these substitutions are still accessible for graphene and should be considered for NPG systems.

For H substitution with =O, –OH and –COOH in NPG, three unique sites were considered (see Table 1 and Figure S1 of the Supporting Information). Graphical representations of all the functionalized NPG systems, together with selected bond lengths, are included in the Supporting Information (Figures S2–S8, Tables S2–S8).

The optimized structures of the O substituted NPG (O-NPG) is shown in Figure 2 (c). In this structure the O atom lies in the plane of NPG with a C=O bond length of 1.26 Å. The substitution of H with OH (OH-NPG) does not alter the structure of the NPG monolayer. In the OH-NPG systems, the H atom of the substituent OH bonded with the nearest C atom of NPG with bond length 1.93 Å. In contrast to the O-NPG and OH-NPG, the COOH-NPG is non-planar since the COOH substituent does not lie in the plane of the NPG monolayer. Due to steric effects, the COOH substituent is situated almost vertically to the plane of the NPG with dihedral angles of 124.7° and 119.4° about the NPG–COOH bond (see Figure 2 (f)).

We now turn our attention to modified NPG in which a C–H group is replaced with an X–H group (X = B, N, P or S). It is important to mention that replacing the carbon atoms at the rim of the pore is energetically more favourable than replacing any of the other carbon atoms in the NPG monolayer. The optimized structure of B doped NPG (B-NPG) is shown in Figure 2 (a). The C–B bond lengths of 1.50 and 1.51 Å are longer than the corresponding C–C bond lengths in pristine NPG (1.39 and 1.41 Å). Similarly, the B–H bond length of 1.20 Å is longer than the C–H bond length of 1.09 Å in the pristine NPG monolayer. Contrary to the B-NPG system, in the N substituted NPG (N-NPG) system, which is shown in Figure 2 (b), the N–C and H–N bond lengths are shortened to 1.37 and 1.01 Å, respectively. In the optimized P- and S-substituted NPG (P-PNG and S-PNG), the P–C, P–H, S–C and S–H bond lengths are found to be 1.74, 1.39, 1.70 and 1.33 Å, respectively. We note that all X-NPG systems are completely planar and that no significant structural deformations are observed as shown in Figure 2 (a, b, d, e).

3.3 Metal adsorption on the functionalized NPG monolayers

Introduction of the substituents or dopants in the NPG systems is expected to affect the electronic structure of the NPG. In this section we study the electronic properties of the functionalized NPG monolayers (FNPG). For this purpose, we have plotted the total density of states (TDOS) plots for all the modified systems (see Figure S9 of the Supporting Information). These plots show that both O-NPG and OH-NPG monolayers display semiconducting behavior with a reduced E_g value of 0.31 eV as compared to 0.63 eV for pristine NPG, whereas all the other modified NPG systems (COOH-NPG, B-NPG, N-NPG, P-NPG, and S-NPG) show metallic character.

We proceed to adsorb metal cations on FNPG structures. Similar to the case of pristine NPG, we have considered all the available binding sites. It is important to mention that for the metal adsorption, we have considered the binding sites in the vicinity as well as away from the substituted functional group/heteroatom dopants in order to probe both localized or delocalized effects on the E_b values of the metal cations. In addition to the available binding sites the binding distances between the metal cations and the FNPG have also been considered. To calculate the adsorption or binding energy the metals on the functionalized NPG, Equation (3) was employed.

$$E_b = E_{M@FNPG} - E_{FNPG} - E_M \qquad (3)$$

Here, the terms on the right-hand side of the equation represents the total energies of metal adsorbed on FNPG (M@FNPG), FNPG, and metal atom (M). The E_b values of the most stable configurations of the metal cations on all systems are given in Figure 3. The binding of the metal cations on each system will be discussed in Sections 3.3.1–3.3.3.

3.3.1 Metal adsorption on O-NPG

In the most stable configurations of metal adsorbed on O-NPG the metal cations Li, Na, K, Mg and Ca are associated with E_b values of -3.30, -2.62, -2.89, -1.67, and -3.40 eV, respectively. These energies are significantly higher than the corresponding E_c values of the metals and the corresponding E_b on pristine NPG (see Tables S1 in Supporting Information). The binding distance (d) of Li, Na, K, Mg, and Ca with O-NPG are found to be 1.75, 2.15, 2.49, 1.93 and 2.10 Å, respectively. We find that the metal cations prefer to bind close to the O-site, within d of 2.5 Å. Optimized structures of metal doped O-NPG are shown in Figure 4. In addition to the binding energies at the sites leading to the strongest adsorption energies, it is useful to look at E_b values at the least favourable adsorption sites in order to probe any delocalized effects of the O dopant. For this purpose, the weakest binding energies ($E_{b,weak}$) are also included in Table S2. The $E_{b,weak}$ values are -3.21 (Li), -2.48 (Na), -2.76 (K), -1.63 (Mg), and -2.96 eV (Ca). The $E_{b,weak}$ values clearly indicate that even at the least preferential binding sites, the metal cations bind fairly strongly to O-NPG. In order to rationalize this delocalized effect it is useful to compare the Bader atomic charges on the carbon atoms surrounding the metal binding site ~10 Å from the O atom with and without the oxygen functionalization. We find that functionalizing with oxygen significantly changes the atomic charges on the carbon atoms even ~10 Å from the oxygen centre. In particular, the atomic charges of these carbons change by up to 0.27 *e* (in absolute value) between the pristine and O-substituted NPG.

In addition to metal binding strength, one also requires a high charge transfer from the metal cations to the FNPG. This has been studied by means of Bader charge analysis. We have found that, in the lowest energy configurations, Bader charges of 0.999, 0.991, 0.901, 1.200 and 1.630 *e* have been transferred to O-NPG from Li, Na, K, Mg, and Ca, respectively. In order to explain the binding at the least favourable adsorption sites, which is at a distance of around 10 Å from the functional group O in O-NPG, we have employed Bader analysis to the metal-doped O-NPG. We have found that relatively smaller amount of charges, 0.992 (Li), 0.989 (Na), 0.810 (K), 1.120 (Mg) and 1.120 *e* (Ca) have been transferred to O-NPG as compared to the most favourable metal binding sites. However, these charges are still greater than the charges transferred from the metal dopants, 0.989 (Li), 0.985 (Na), 0.803 (K), 1.080 (Mg) and 1.060 (Ca) to the pristine NPG. The change in the charge concentration of O-NPG is associated with the alteration in its electronic structure, as shown in the DOS plots. Figure S2 (Supplementary Information) shows the TDOS plots of O-NPG with the adsorbed metal cations in their lowest energy configurations. It is evident from Figure S10 that all systems show metallic character, which is desired for efficient anode materials. In addition, the

transfer of charge from the metal cations to O-NPG results in ionic bonding, which has been further verified by means of Roby-Gould bond index methods as shown in Figure S16 (Supporting Information).

In addition to Bader analysis, we have also studied the charge transfer by using Roby-Gould bond indices (RGBIs). **[57-60]** This method is used to estimate the percentage ionicity (i.e. amount of charge transfer) for the bonds between the metal cations to the FNPG (see Figure S16 of the Supporting Information). The RGBI method calculates two bond indices, the covalent (c) and ionic (i) index. The total RGBI bond index can be then defined by using these two indices, as follows,

$$\tau = \sqrt{c^2 - i^2}.$$

The percentage ionicity (%I) of O-NPG-dopants is given as,

$$\%\mathrm{I} = (100)\,\frac{i^2}{\tau^2}.$$

For convenience, we have presented the %I values of metal cations to the O-NPG, which were found as 88, 72, 83, 42, and 67% for Li, Na, K, Mg, and Ca, respectively. These values are further demonstrated by plotting the RGBI ionic states (Figure S16), which show the accumulation and depletion of the charge density around O-NPG and dopants, respectively. We observed strong ionic characters of the metal cations bonded to the other FNPG systems.

3.3.2 Metal adsorption on COOH-NPG

Similarly to O-NPG, COOH-NPG improves the E_b values of all the metal cations. In the lowest energy configurations, the E_b values of Li, Na, K, Mg, and Ca on COOH-NPG are -2.13, -1.53, -1.83, -2.40 and -2.26 eV, respectively (Table S2, Supporting Information). Although the E_b values are weaker than that of the O-NPG system, they are still stronger than those on pristine NPG as well as than the corresponding E_c values of the metal cations. The ◘d for the most stable configurations, as shown in Figure 5, are 1.84, 2.19, 2.58, 3.09 and 2.24 Å for Li, Na, K, Mg and Ca, respectively. All of the metal cations prefer to bind with the carbonyl oxygen of COOH with binding distances of 1.85 (Li), 2.19 (Na), 2.85 (K), 3.07 (Mg), and 2.24 (Ca) Å. It is noted that unlike O-NPG, the COOH-NPG system does not improve the E_b values of all the configurations. For example, we obtain $E_{b,weak}$ values of -1.41 (Li), -0.88 (Na), -1.37 (K), -0.22 (Mg) and -1.05 eV (Ca) which are weaker than in the most stable configurations, indicating that COOH substituent only has a local effect on the metal binding. Moreover, we note that these $E_{b,weak}$ values are weaker than the corresponding E_c

values except for K. Bader charge analysis reveals that the amount of charges transferred to COOH-NPG by Li, Na, K, Mg and Ca are 0.997, 0.992, 0.905, 1.25 and 1.54 *e*, respectively. The TDOS plots of the COOH-NPG systems bonded with the metal cations in their most stable configurations are shown in Figure S11 (Supplementary Information). From Figures S10 and S11 it is evident that, similar to O-NPG, the COOH-NPG systems become metallic upon the adsorption of metal cations.

3.3.3 Metal adsorption on OH-NPG

In the case of OH-NPG, there is little or no improvement in E_b values for Li, K, and Mg cations compared to the pristine NPG systems. In the ground state configurations, the E_b values for Li, Na, K, Mg, and Ca are found to be -1.48, -0.96, -1.32, -0.35, and -1.27 eV, respectively. These E_b values for Na and Ca represent only a small increment as compared to pristine NPG. However, these E_b values are lower than the E_c values of Na (-1.11) and Ca (-1.84 eV). Similarly, the $E_{b,weak}$ values for Li, Na, K, Mg, and Ca are weaker than the E_c values of these metal dopants as shown in Table S1 (Supporting Information). These results suggest that OH-NPG is not an efficient anode material and therefore it is not discussed further.

3.4 Metal adsorption on doped X-NPG monolayers (X = B, N, P, S)

In the previous sections we considered functionalized NPG systems in which hydrogens are substituted with oxygen-containing functional groups (O-NPG, OH-NPG, and COOH-NPG). In this section we turn our attention to doped NPG systems in which a carbon atom is replaced with an heteroatom (X-NPG; X = B, N, P, and S).

3.4.1 Metal adsorption on B-NPG

The E_b values of the considered metals on B-NPG in the most stable configurations are presented in Figure 3, whilst the structures are shown in Figure 6. With the exception of Mg, the binding energies of all metal cations are stronger relative to pristine NPG. Specifically, the E_b values on B-NPG are -2.69, -2.26, -2.36, -0.89, and -2.28 eV for Li, Na, K, Mg, and Ca, respectively. It is evident from Table S2 (Supplementary Information) that the ratio $E_b/E_c > 1$ for all metal cations except Mg, indicating that these metals would bind to B-NPG without metal clustering. The bonding distances d for Li, Na, K, Mg, and Ca are 2.17, 2.55, 2.94, 3.05, and 2.58 Å, respectively. Similar to the substituted FNPG systems, the metal cations prefer to bind with B-NPG in the vicinity of the B atom (within 3 Å). Although we find an improvement in the E_b values of the metal cations for the other configurations, the

$E_{b,weak}$ which is resulted at a distance of 10 Å from the substituent B_C, for Li (-1.52), Na (-1.01), Mg (-0.25), and Ca (-0.97 eV) fall short of their corresponding E_c values as shown in table S1 (Supporting Information). The binding sites in close vicinity of the B atom are more promising in improving the binding of the metal cations in B-NPG system. Thus, the effect of the B dopant seems to be localized and becomes weaker as the metal cations binds further away from it. It is found that Li, Na, K, Mg, and Ca have transferred charges of 0.989, 0.967, 0.888, 0.140, and 1.100 *e* to B-NPG, respectively. Charge transfer does not alter the metallic character of the B-NPG system without metal adatoms and all B-NPG systems with adsorbed metals show metallic properties as shown in the TDOS plots in Figure S12 (Supporting Information).

3.4.2 Metal adsorption on N-NPG

The improvement in E_b of metal cations on N-NPG as compared to pristine NPG is smaller than that in B-NPG. The optimal E_b values on N-NPG are -1.98, -1.38, -1.84, -0.90, and -1.68 eV, for Li, Na, K, Mg, and Ca, respectively. These E_b values are stronger than the metal clustering energies for Li, Na, and K, whereas for Mg and Ca metal clustering is energetically favourable (Table S1, Supporting Information). This suggests that N-NPG is not suitable as an anode material in MIBs and CIBs, where cluster formation would be favourable and limit battery performance. The lowest energy configurations are associated with d values of 2.03, 2.42, 2.97, 2.98, and 2.45 Å for Li, Na, K, Mg, and Ca, respectively. It is worth mentioning that as can be seen from Figure 7, Li, Na, and Ca bind in the vicinity of the dopant N within a binding distance of around 3 Å, whereas K and Mg bind further away (10 and 4 Å, respectively). The $E_{b,weak}$ values of Li (-1.64), Na (-1.12), K (-1.67), Mg (-0.74) and Ca (-1.23 eV) show that the N-NPG systems could be used for Li, Na, and K. Bader charge analysis shows that charges of 0.988, 0.985, 0.899, 0.171, and 0.950 *e* have been transferred to N-NPG from Li, Na, K, Mg, and Ca, respectively. The electronic structure of N-NPG with adsorbed metal cations was evaluated in terms of TDOS plots. As can be seen from Figure S13 (Supporting Information) all systems are metallic.

3.4.3 Metal adsorption on P-NPG

The P-NPG monolayer is found to be one of the best systems for binding metal cations among the functionalized NPG systems investigated in this study. There is a large increase in E_b for all the metal cations upon the formation of a P defect. The calculated E_b for the lowest energy configurations of Li, Na, K, Mg, and Ca are -3.33, -2.37, -2.79, -1.53, and -3.20 eV,

respectively, and the structures are given in Figure 8. These E_b values are comparable to the O-NPG systems and are much stronger than those on pristine NPG. Furthermore, the P defect is more beneficial for metal binding than both (i) doping with B or N, and (ii) substitution with the OH or COOH functional groups. For all the metal cations, $E_b/E_c > 1$, which indicates the metal bindings are more favorable than the metal clustering as evident in Table S1 (Supporting Information). We observe that the metal cations prefer to bind close to P with ◘d of 2.16, 2.52, 2.86, 2.55, and 2.54 Å for Li, Na, K, Mg, and Ca, respectively. The calculated $E_{b,weak}$ values of -2.30 (Li), -1.75 (Na), -2.25 (K), -1.11 (Mg), and -1.84 eV (Ca) suggest that the metal cations bind efficiently to P-NPG with the exception of Mg even at the least preferred binding sites. Major portion of the electronic charges are transferred from Li (0.990), Na (0.988), K (0.857), Mg (1.23), and Ca (1.36) to the P-NPG. TDOS plots of P-NPG with metal adsorbents show a metallic character as shown in Figure S14 (Supporting Information).

3.4.4 Metal adsorption on S-NPG

Finally, the binding of metal cations with an S-doped NPG is studied. The energetic analysis reveals that the S dopant leads to the largest increase in E_b for all metal cations. The lowest energy configurations yield E_b values of -3.87, -3.28, -3.37, -3.68, and -4.97 eV for Li, Na, K, Mg, and Ca, respectively. It is clearly seen that the S defect improves E_b more than all the other defects presented in Section 3.2, and presents a marked increase in metal binding as compared to pristine NPG. The ◘d for Li, Na, K, Mg and Ca are 2.20, 2.69, 3.10, 2.55m, and 2.72 Å, respectively. In addition, the effect of the S defect is not localized, which is evident from $E_{b,weak}$ values of -2.48 (Li), -2.00 (Na), -3.01 (K), -2.33 (Mg), and -2.46 eV (Ca) as given in Table S1 (Supporting Information). Interestingly the change in the structural properties of S-NPG are more pronounced than the other functionalized NPG systems upon the introduction of metal cations. Unlike S-NPG which is planar, in all M@S-NPG systems (M = Li, Na, K, Mg, and Ca) the S atom is situated 0.3–0.5 Å below the plane of the S-NPG plane as shown in Figure 9. This structural rearrangement changes the C–S–C angle from 113.0° in S-NPG to 102.5, 102.7, 102.6, 90.0 and 96.6° for Li, Na, K, Mg and Ca, in M@S-NPG, respectively. Bader charge analysis shows the following charge transfer from M to S-NPG 0.984 (Li), 0.981 (Na), 0.836 (K), 1.48 (Mg) and 1.36 *e* (Ca). Due to the pronounced structural changes of S-NPG upon metal binding it is of interest to examine the thermal stability of the S-NPG monolayer. We have done this by means of ab initio molecular dynamics (AIMD) simulations, which show that S-NPG remains stable at temperatures of up to 400 K (see Figure S17 of the Supporting Information).

Upon metal adsorption the S-NPG monolayer remains metallic as confirmed by TDOS plot in Figure S15 (Supporting Information). We note that the binding energy for Li falls outside the common range for anode materials, which should result in a high operational voltage for S-NPG. However, it is important to note that the binding energies of Li over the other functionalized NPG monolayers are within the common range for anode materials application, namely: -2.69 (B-NPG), -1.98 (N-NPG), and -2.13 (COOH-NPG) eV.

4. Conclusion

The recent synthesis of the novel 2D nanoporous graphene (NPG) monolayer has generated interest due to its exceptional structural, electronic and thermal properties. Motivated by these intriguing properties, we used dispersion-corrected DFT calculations to study the structural, defect formation, electronic structure, metal binding, and charge transfer properties of NPG monolayers. Calculation of metal binding energies revealed that pristine NPG could not bind the metal cations strongly enough to warrant their use as efficient anode materials for metal ion batteries. However, the substitution of various functional groups (O, OH, COOH) and different metal dopants (B, N, P, S) enhanced the metal binding properties of the NPG monolayers. The metal binding energies were improved as $S_C > P_C > O_H > B_C > N_C > (COOH)_H > (OH)_H$. In addition to strong metal binding, large charge transfer from the metal cations to the NPG monolayers is beneficial for battery applications. To study the charge transfer, Bader charge analysis and Roby-Gould bond index methods were employed. This analysis showed the ionic nature of the metal dopants through the transfer of their charges to the NPG systems. The electronic properties of pristine and defective NPG were studied by plotting their density of states. After the introduction of metal cations, all the functionalized systems showed metallic character, which is highly desirable for these anode materials. These findings show that these materials are promising MIB anode candidates due of their strong metal binding and metallic nature, which is capable of robust charge transfer properties. It is our belief that this first computational study will pave the way for the optimization of NPG as an efficient anode material for Li, Na, K, Mg and Ca ion rechargeable batteries.

Authors contributions statement:

Tanveer Hussain: Conceptualization, Data curation, Writing- Original draft preparation. Khidhir Alhameedi: Visualization, Investigation. Qiong Cai, Amir

Karton: Supervision. Emilia Olsson: Software, Validation. Tanveer Hussain, Emilia Olsson, Amir Karton, Qiong Cai: Writing- Reviewing and Editing,

Acknowledgements

This research was undertaken with the assistance of resources from the National Computational Infrastructure (NCI), which is supported by the Australian Government. This work was also supported by resources provided by the Pawsey Supercomputing Centre with funding from the Australian Government and the Government of Western Australia. AK acknowledges an Australian Research Council (ARC) Future Fellowship (FT170100373). EO and QC would like to acknowledge the financial support from EPSRC (Engineering and Physical Sciences Council) under grant number EP/P003354/1 and EP/R021554/1. We acknowledge the use of Athena at HPC Midlands+, which was funded by the EPSRC on grant EP/P020232/1, in this research, and the Eureka HPC cluster at the University of Surrey. *Via* our membership of the UK's HEC Materials Chemistry Consortium, which is funded by EPSRC (EP/L000202), this work used the UK Materials and Molecular Modelling Hub for computational resources, MMM Hub, which is partially funded by EPSRC (EP/P020194).

References

1. M. A. Hannan, M. M. Hoque, A. Mohammad, A. Ayob, Review of energy storage systems for electric vehicle applications: Issues and challenges. *Ren. Sustain. Energy Rev*. **69**, 771-789 (2017) doi.org/10.1016/j.rser.2016.11.171

2. P. K. Nayak, L. Yang, W. Brehm, P. Adelhelm. From Lithium-Ion to Sodium-Ion Batteries: Advantages, Challenges, and Surprises. *Ang. Chem. Int. Ed*. **57**, 102-120 (2017) doi.org/10.1002/anie.201703772

3. A. H. F. Niaei, T. Hussain, M. Hankel, D. J. Searles, Hydrogenated defective graphene as an anode material for sodium and calcium ion batteries: A density functional theory study. *Carbon* **136**, 73-84 (2018) doi.org/10.1016/j.carbon.2018.04.034

4. H. Zhang, I. Hasa, S. Passerini. Beyond Insertion for Na-Ion Batteries: Nanostructured Alloying and Conversion Anode Materials. *Adv. Energy Mater.* 8, 1702582-1702621 (2018) DOI: 10.1002/aenm.201702582

5. J. Qian, C. Wu, Y. Cao, Z. Ma, Y. Huang, X. Ai, H. Yang. Prussian Blue Cathode Materials for Sodium-Ion Batteries and Other Ion Batteries. *Adv. Energy Mater.* **8**, 1702619-1702644 (2018) doi.org/10.1002/aenm.201702619

6. B. Mortazavi, O. Rahaman, S. Ahzi, T. Rabczuk. Flat borophene films as anode materials for Mg, Na or Li-ion batteries with ultrahigh capacities: A first-principles study. *App. Mater. Today* **8**, 60-67 (2017) doi.org/10.1016/j.apmt.2017.04.010

7. G. Assat, J-M. Tarascon. Fundamental understanding and practical challenges of anionic redox activity in Li-ion batteries. *Nature Energy* **3**, 373-386 (2018) DOI: 10.1038/s41560-018-0097-0

8. P-F. Wang, H-R. Yao, H-Y. Liu, Y-X. Yin, J-N. Zhang, Y. Wen, X. Yu, L. Gu, Y-G. Guo. Na^+/vacancy disordering promises high-rate Na-ion batteries. *Sci. Adv*. **4**, eaar6018 (2018) doi: 10.1126/sciadv.aar6018

9. W. Wang, J. Zhou, Z. Wang, L. Zhao, P. Li, Y. Yang, C. Yang, H. Huang, S. Guo, Short‐Range Order in Mesoporous Carbon Boosts Potassium‐Ion Battery Performance. *Adv. Energy Mater.* 8, 1701648-1701655 (2018) doi.org/10.1002/aenm.201701648

10. T. R. Juran, M. Smeu, Hybrid density functional theory modeling of Ca, Zn, and Al ion batteries using the Chevrel phase Mo6S8 cathode. *Phys. Chem. Phys. Chem*. **19**, 20684-20690 (2017) DOI: 10.1039/c7cp03378h

11. A. H. F. Niaei, T. Roman, T. Hussain, D. J. Searles, Computational Study on the Adsorption of Sodium and Calcium on Edge-Functionalized Graphene Nanoribbons. *J. Phys. Chem. C* **123**, 14895-14908 (2019) doi.org/10.1021/acs.jpcc.9b02003

12. Z. Yao, V. I. Hegde, A. Aspuru-Guzik, C. Wolverton, Discovery of Calcium-Metal Alloy Anodes for Reversible Ca-Ion Batteries. *Adv. Energy Mater.* **9**, 1802994-1803003 (2019) doi.org/10.1002/aenm.201802994

13. Q. Fu, A. Sarapulova, V. Trouillet, L. Zhu, F. Fauth, S. Mangold, E. Welter, S. Indris, M. Knapp, S. Dsoke, N. Bramnik, H. Ehrenberg. In Operando Synchrotron Diffraction and in Operando X-ray Absorption Spectroscopy Investigations of Orthorhombic V_2O_5 Nanowires as Cathode Materials for Mg-Ion Batteries. *J. Am. Chem. Soc*. **141**, 2305-2315 (2019) doi.org/10.1021/jacs.8b08998

14. A. Ponrouch, C. Frontera, F. Bardé, M. R. Palacin, Towards a calcium-based rechargeable battery. *Nat. Mater*. **15**, 169-172 (2016) doi.org/10.1038/nmat4462

15. A. Samad, A. Shafique, Y-H. Shin, Adsorption and diffusion of mono, di, and trivalent ions on two-dimensional TiS_2. *Nanotechnology* **28**, 175401-175407 (2017) DOI: 10.1088/1361-6528/aa6536

16. Y. Zeng, X. Zhang, R. Qin, X. Liu, P. Fang, D. Zheng, Y. Tong, X. Lu, Dendrite-Free Zinc Deposition Induced by Multifunctional CNT Frameworks for Stable Flexible Zn-

Ion Batteries. *Adv. Mater*. **31**, 1903675-1903682 (2019) doi.org/10.1002/adma.201903675

17. A. Ponrouch, J. Bitenc, R. Dominko, N. Lindahl, P. Johansson, M. R. Palacin, Multivalent rechargeable batteries. *Ener. Stor. Mater*. **20**, 253-262 (2019) doi.org/10.1016/j.ensm.2019.04.012
18. X. Sun, P. Bonnick, V. Duffort , M. Liu , Z. Rong , K. A. Persson , G. Ceder, L. F. Nazar, A high capacity thiospinel cathode for Mg batteries. *Energy Environ. Sci.* **9**, 2273-2277 (2016) DOI: 10.1039/C6EE00724D
19. A. H. F. Niaei, T. Hussain, M. Hankel, D. J. Searles, Sodium-intercalated bulk graphdiyne as an anode material for rechargeable batteries. *J. Power Sources*, **343**, 354-363 (2017) doi.org/10.1016/j.jpowsour.2017.01.027
20. X. Deny, X. Chen, Y. Huang, B. Xiao, H. Du, Two-Dimensional GeP_3 as a High Capacity Anode Material for Non-Lithium-Ion Batteries. *J. Phys. Chem. C* **123**, 4721-4728 (2019) doi.org/10.1021/acs.jpcc.8b11574
21. F. Bonaccorso, Z. Sun, T. Hasan, A. C. Ferrari, Graphene photonics and optoelectronics. *Nat. Photonics* **4**, 611-622 (2010) doi.org/10.1038/nphoton.2010.186
22. M. Liu, X. Yin, E. Ulin-Avila, B. Geng, T. Zentgraf, L. Ju, F. Wang, X. Zhang, A graphene-based broadband optical modulator. *Nature* **474**, 64-67 (2011) doi.org/10.1038/nature10067
23. A. Allahbakhsh, M. Arjmand, Graphene-based phase change composites for energy harvesting and storage: State of the art and future prospects. *Carbon* **148**, 441-480 (2019) doi.org/10.1016/j.carbon.2019.04.009
24. F. Zhan, Z. Wang, T. Wu, Q. Dong, C. Zhao, G. Wang, J. Qiu, High performance concentration capacitors with graphene hydrogel electrodes for harvesting salinity gradient energy. *J. Mat. Chem. A* **6**, 4981-4987 (2018) DOI: 10.1039/C7TA11070G
25. J. Yang, X. Zhou, D. Wu, X. Zhao, Z. Zhou, S-Doped N-Rich Carbon Nanosheets with Expanded Interlayer Distance as Anode Materials for Sodium-Ion Batteries. *Adv. Mater*. **29**, 1604108-1604112 (2017) DOI: 10.1002/adma.201604108
26. H. Tabassum, C. Zhi, T. Hussain, T. Qiu, W. Aftab, R. Zou, Encapsulating Trogtalite $CoSe_2$ Nanobuds into BCN Nanotubes as High Storage Capacity Sodium Ion Battery Anodes. *Adv. Energy Mater*. 1901778-1901787 (2019) DOI: 10.1002/aenm.201901778
27. R. Fang, K. Chen, L. Yin, Z. Sun, F. Li, H-M. Cheng, The Regulating Role of Carbon Nanotubes and Graphene in Lithium-Ion and Lithium–Sulfur Batteries. *Adv. Mater*. **31**, 1800863-1800884 (2019) DOI: 10.1002/adma.201800863

28. K. Share, A. P. Cohn, R. Carter, B. Rogers, C. L. Paint, Role of Nitrogen-Doped Graphene for Improved High-Capacity Potassium Ion Battery Anodes. *ACS Nano* **10**, 9738-9744 (2016) DOI: 10.1021/acsnano.6b05998
29. D. Datta, J. Li, V. B. Shenoy, Defective Graphene as a High-Capacity Anode Material for Na- and Ca-Ion Batteries. *ACS Appl. Mater. Interfaces* **6,** 1788□1795 (2014) doi.org/10.1021/am404788e
30. B. Mortazavi, M. Shahrokhi, X. Zhuang, T. Rabczuk. Boron–graphdiyne: a superstretchable semiconductor with low thermal conductivity and ultrahigh capacity for Li, Na and Ca ion storage. *J. Mater. Chem. A* **6**, 11022-11036 (2018) DOI: 10.1039/C8TA02627K
31. K. Wang, N. Wang, J. He, Z. Yang, X. Shen, C. Huang, Preparation of 3D Architecture Graphdiyne Nanosheets for High-Performance Sodium-Ion Batteries and Capacitors. *ACS Appl. Mater. Interfaces* **9,** 40604□40613 (2017) DOI: 10.1021/acsami.7b11420
32. M. Hankel, D. J. Searles, Lithium storage on carbon nitride, graphenylene and inorganic graphenylene. *Phys. Chem. Chem. Phys*. **18**, 24205-24215 (2016) DOI: 10.1039/C5CP07356A
33. D. Ferguson, D. J. Searles, M. Hankel, Biphenylene and Phagraphene as Lithium Ion Battery Anode Materials. *ACS Appl. Mater. Interfaces* **9**, 20577□20584 (2017) DOI: 10.1021/acsami.7b04170
34. P. Bhauriyal, A. Mahata, B. Pathak, Graphene-like Carbon□Nitride Monolayer: A Potential Anode Material for Na- and K□Ion Batteries. *J. Phys. Chem. C* **122**, 2481-2489 (2018) DOI: 10.1021/acs.jpcc.7b09433
35. M. Hankel, D. Ye, L. Wang, D. J. Searles, Lithium and Sodium Storage on Graphitic Carbon Nitride. *J. Phys. Chem. C* **119**, 21921-21927 (2015) DOI: 10.1021/acs.jpcc.5b07572
36. K. Celebi, J. Buchheim, R. R. Wyss, A. Droudian, P. Gasser, I. Shorubalko, J. Kye, C. Lee, H. G. Park, Ultimate Permeation Across Atomically Thin Porous Graphene. *Science* **344**, 289-292 (2014) DOI: 10.1126/science.1249097
37. R. H. Scheicher, A. Grigoriev, R. Ahuja, DNA sequencing with nanopores from an ab initio perspective, *J. Mater. Sci*. **47**, 7439-7446 (2012) doi.org/10.1007/s10853-012-6671-0.
38. C. Sun, B. Wen, B. Bai, Application of nanoporous graphene membranes in natural gas processing: Molecular simulations of CH_4/CO_2, CH_4/H_2S and CH_4/N_2 separation. *Chem. Eng. Sci*. **138**, 616-621 (2018)
39. A. W. Hauser, P. Schwerdtfeger, Nanoporous Graphene Membranes for Efficient $^3He/^4He$ Separation. *J. Phys. Chem. Lett*. **3,** 209-2013 (2012)
40. C. Moreno, M. Vilas-Varela, B. Kretz, A. Garcia-Lekue, M.V. Costache, M. Paradinas, M. Panighel, G. Ceballos, S.O. Valenzuela, D. Pena, A. Mugarza, Bottom-up synthesis of multifunctional nanoporous graphene, *Science* **360**, 199-203 (2018), doi.org/10.1126/science.aar2009
41. B. Mortazavi, M. E. Madjet, M. Shahrokhi, S. Ahzi, X. Zhuang, T. Rabczuk, Nanoporous graphene: A 2D semiconductor with anisotropic mechanical, optical and thermal

conduction properties. *Carbon* **147**, 277-384 (2019) doi.org/10.1016/j.carbon.2019.03.018
42. G. Kresse, J. Hafner, Ab initio molecular dynamics for liquid metals. *Phys. Rev. B* **47**, 558-561 (1993) doi.org/10.1103/PhysRevB.47.558
43. G. Kresse, J. Hafner, Ab initio molecular-dynamics simulation of the liquid-metal–amorphous-semiconductor transition in germanium. *Phys. Rev. B* **49** 14251-14269 (1994) doi.org/10.1103/PhysRevB.49.14251
44. J. P. Perdew, K. Burke, M. Ernzerhof, Generalized gradient approximation made simple. *Phys. Rev. Lett.* **77**, 3865-3868 (1996) DOI:10.1103/PhysRevLett.77.3865
45. P. E. Blochl, Projector augmented-wave method. *Phys. Rev. B* **50**, 17953-17979 (1994) doi.org/10.1103/PhysRevB.50.17953
46. S. Grimme, J. Antony, S. Ehrlich, H. Krieg, A consistent and accurate ab initio parametrization of density functional dispersion correction (DFT-D) for the 94 elements H–Pu. *J. Chem. Phys.* **132**, 154104-154119 (2010) doi.org/10.1063/1.3382344
47. H. J. Monkhorst, J. D. Pack, Special points for Brillouin-zone integrations. *Phys. Rev. B* **13**, 5188-5192 (1976) doi.org/10.1103/PhysRevB.13.5188
48. R. F. W. Bader, Atoms in Molecules - a Quantum Theory, Oxford University Press, Oxford**, 1990.**
49. Y-X. Yu, Graphenylene: a Promising Anode Material for Lithium-ion Batteries with High Mobility and Storage. *J. Mater. Chem. A* **1**, 13559□13566 (2013) DOI: 10.1039/C3TA12639K
50. T. Hussain, M. Hankel, D. J. Searles, Graphenylene Monolayers Doped with Alkali or Alkaline Earth Metals: Promising Materials for Clean Energy Storage. *J. Phys. Chem. C* 121, 14393-14400 (2017) DOI: 10.1021/acs.jpcc.7b02191
51. K. Lee, E. D. Murray, L. Kong, B. I. Lundqvist, D. C. Langreth, Higher-Accuracy Van der Waals Density Functional. *Phys. Rev. B* **82**, 081101-081104 (2010) doi.org/10.1103/PhysRevB.82.081101
52. S. B. Zhang, J. E. Northrup, Chemical potential dependence of defect formation energies in GaAs: Application to Ga self-diffusion. *Phys. Rev. Lett*. **67**, 2339-2342 (1991) DOI:10.1103/PhysRevLett.67.2339
53. E. Olsson, G. Chai, M. Dove, Q. Cai, Adsorption and migration of alkali metals (Li, Na, and K) on pristine and defective graphene surfaces. *Nanoscale* **11**, 5274-5284 (2019) DOI: 10.1039/C8NR10383F
54. Y. S. Yun, V-D. Le, H. Kim, S-J. Chang, S. J. Baek, S. Park, B. H. Kim, Y-H. Kim, K. Kang, H-J. Jin, Effects of sulfur doping on graphene-based nanosheets for use asanode materials in lithium-ion batteries. *J. Power Sources*, **262**, 79-85 (2014) doi.org/10.1016/j.jpowsour.2014.03.084
55. E. Cruz-Silva, Z. M. Barnett, B. G. Sumpter, V. Meunier, Structural, magnetic, and transport properties of substitutionally doped graphene nanoribbons

from first principles. Phys. Rev. B 83, 155445-155453 (2011) doi.org/10.1103/PhysRevB.83.155445
56. P. A. Denis, Band gap opening of monolayer and bilayer graphene doped with aluminium, silicon, phosphorus, and sulfur. Chem. Phys. Lett. 492, 251-257 (2010) doi.org/10.1016/j.cplett.2010.04.038
57. M. D. Gould, C. Taylor, S. K. Wolff, G. S Chandler, D. Jayatilaka, D. (2008). A definition for the covalent and ionic bond index in a molecule. *Theoretical Chemistry Accounts*, *119*(1-3), 275-290 (2008) doi.org/10.1007/s00214-007-0282-x
58. K. Alhameedi, B. Bohman, A. Karton, D. Jayatilaka, Predicting the primary fragments in mass spectrometry using ab initio Roby–Gould bond indices. *Int. J. Quantum Chem. 118*, e25603 (2018) doi.org/10.1002/qua.25603
59. K. Alhameedi, A., Karton, D., Jayatilaka, S. P. Thomas, Bond orders for intermolecular interactions in crystals: charge transfer, ionicity and the effect on intramolecular bonds. *IUCrJ*, *5*, 635-646 (2018) doi.org/10.1107/S2052252518010758
60. K. Alhameedi, T., Hussain, H., Bae, D., Jayatilaka, H, Lee, A. Karton, Reversible hydrogen storage properties of defect-engineered C4N nanosheets under ambient conditions. *Carbon* **152**, 344-353 (2019) doi.org/10.1016/j.carbon.2019.05.080

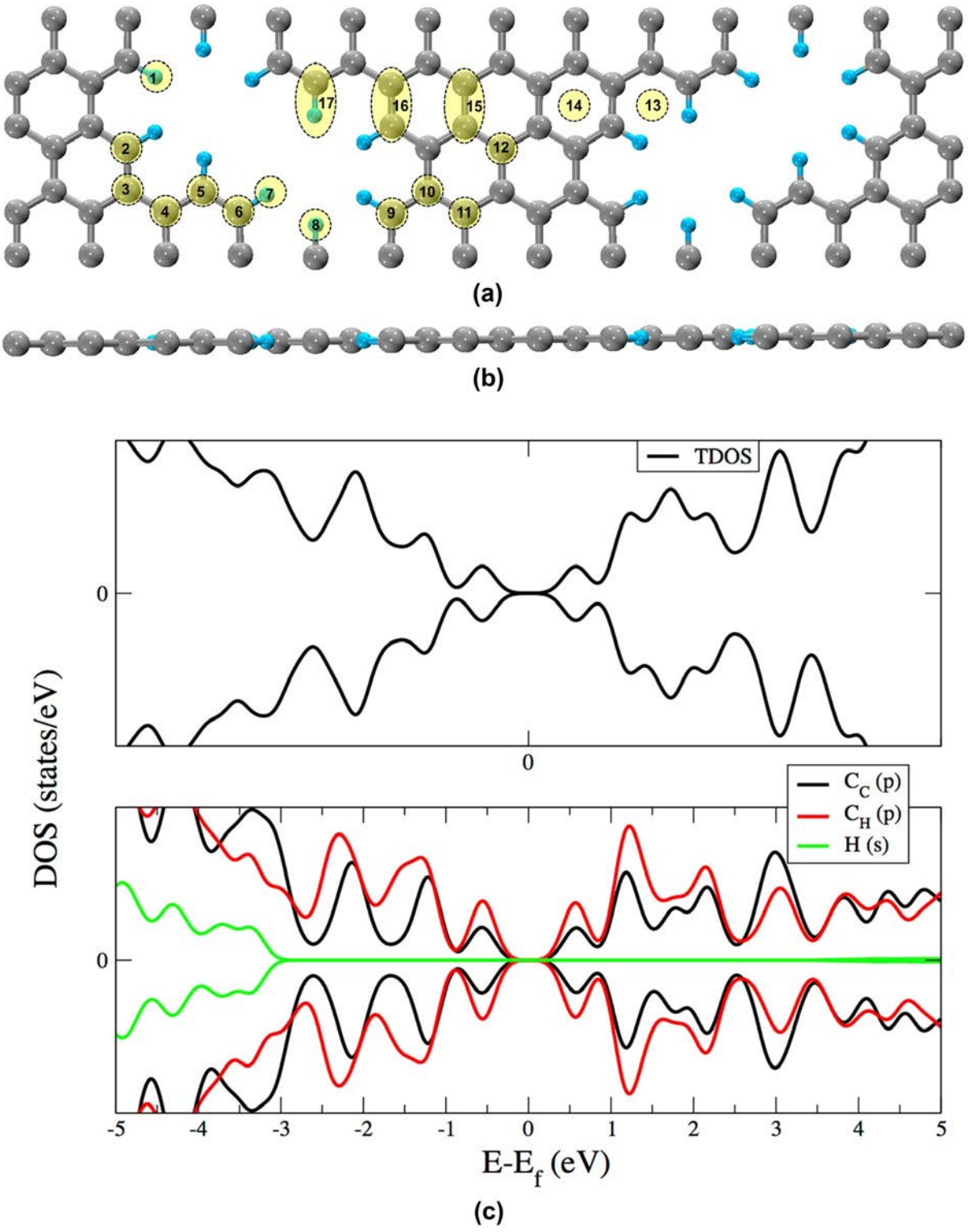

Figure 1: Top (a) and side (b) views of the optimized structures of the NPG monolayer, (c) TDOS (upper panel) and PDOS (lower panel) of pristine NPG monolayer. Grey and blue balls represent C and H atoms, respectively. The various possible metal binding sites are labeled in (a) using numbers 1-17.

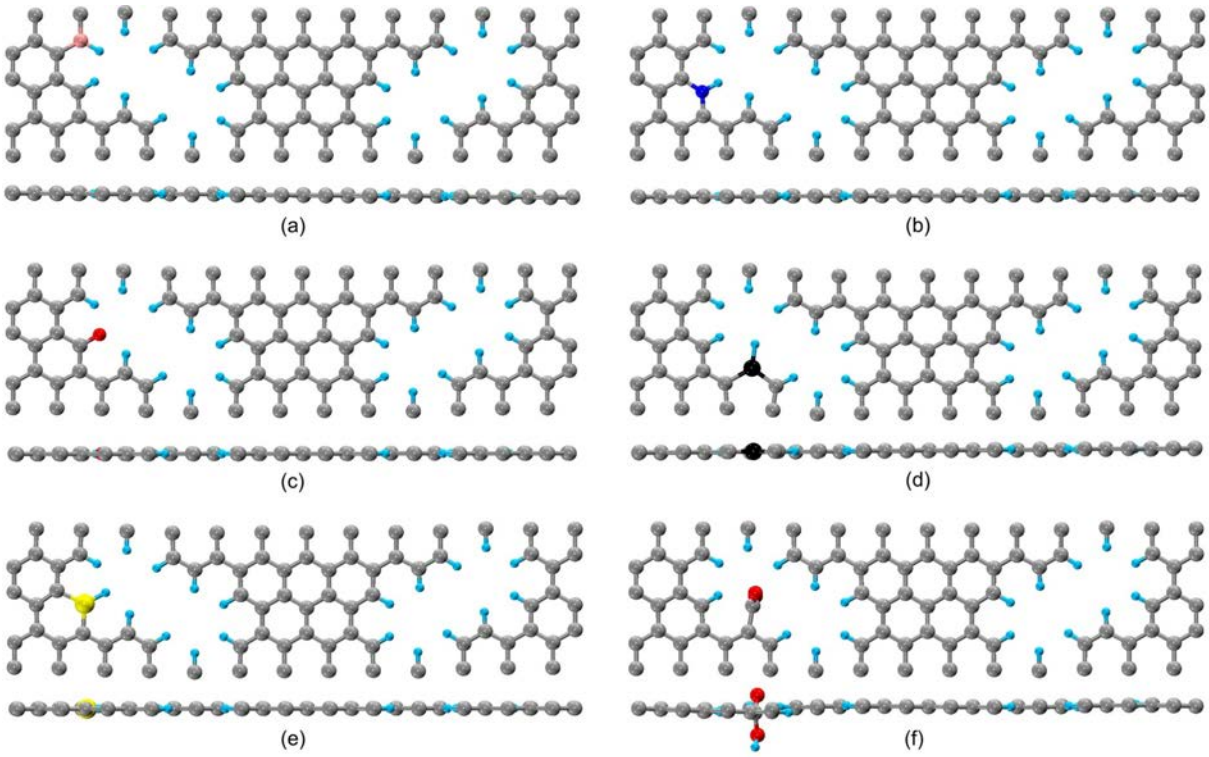

Figure 2: Top and side views of the optimized structures of (a) B-NPG (b) N-NPG (c) O-NPG (d) P-NPG (e) S-NPG and, (f) COOH-NPG. Grey, blue, orange, dark blue, red, black, and yellow balls represent C, H, B, N, O, P and S atoms, respectively.

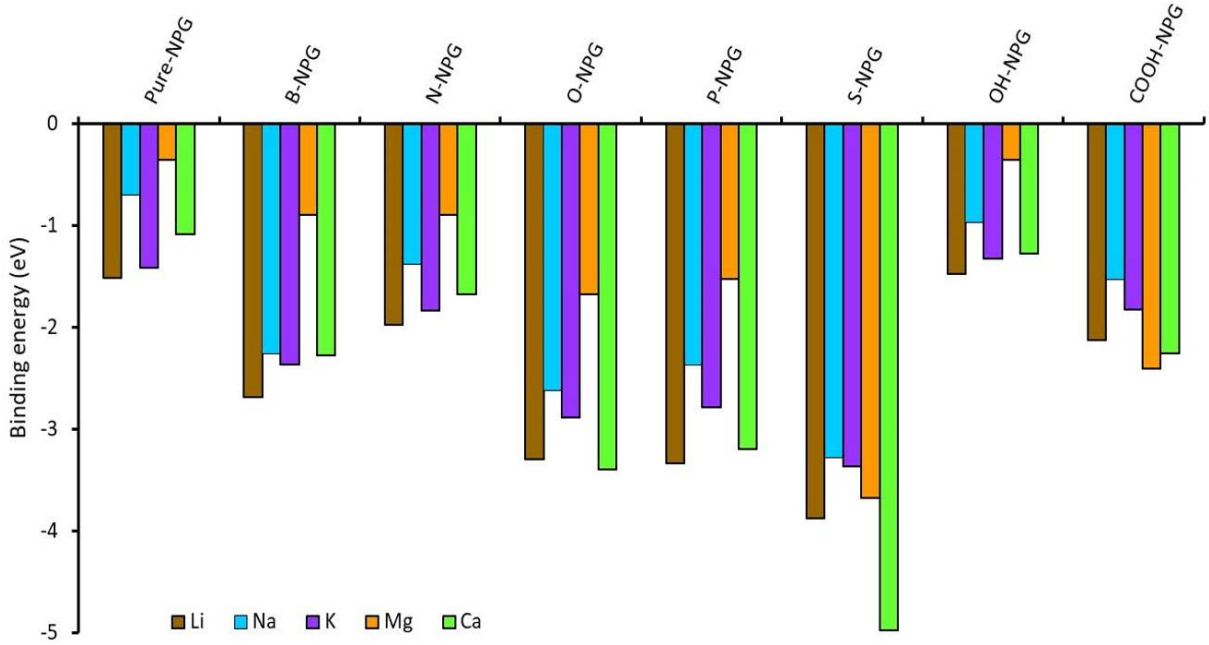

Figure 3: Adsorption energies (E_{ads}) of the most stable configurations of Li, Na, K, Mg and Ca on pristine and functionalized NPG systems.

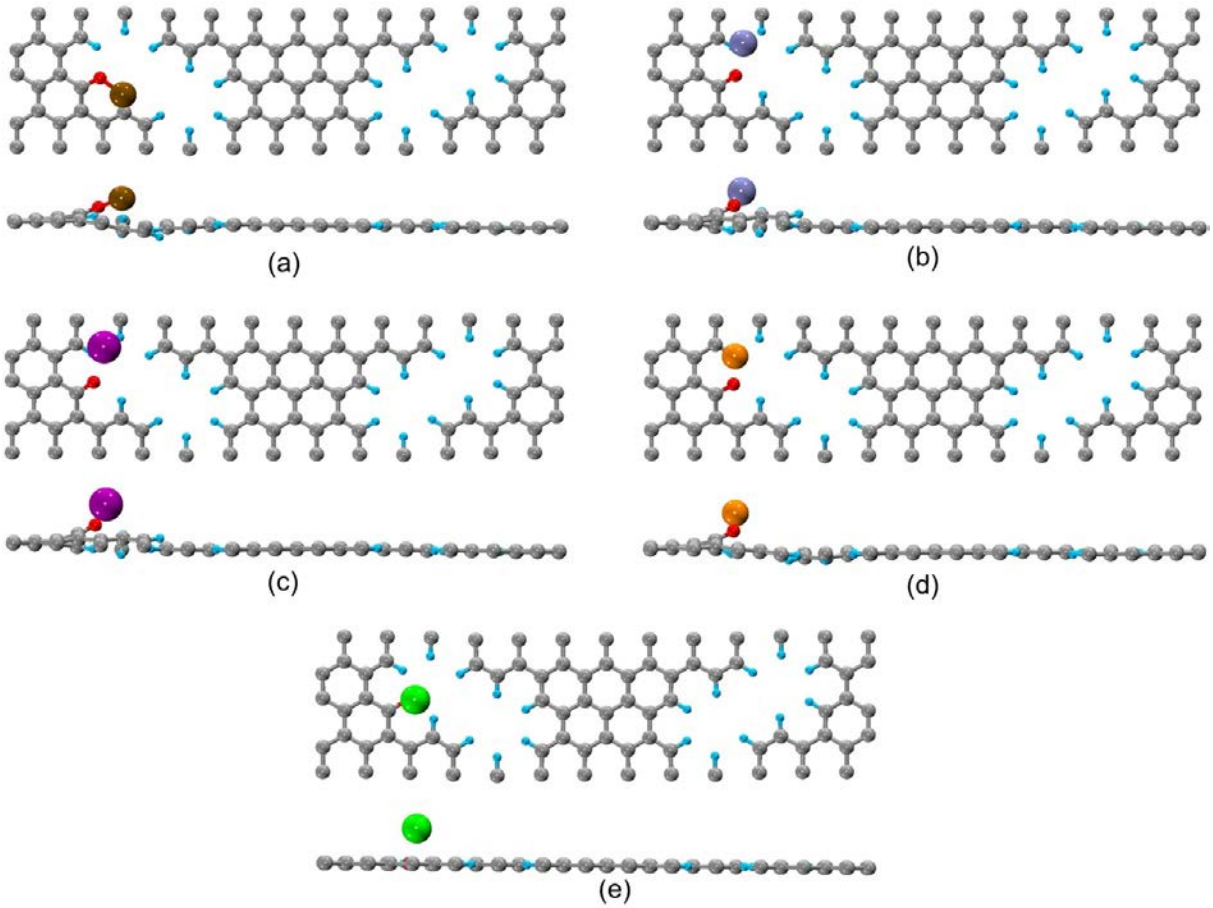

Figure 4: Top and side views of the optimized structures of (a) Li@O-NPG (b) Na@O-NPG (c) K@O-NPG (d) Mg@O-NPG and (e) Ca@O-NPG. Grey, blue, red, brown, purple, magenta, orange and green balls represent C, H, O, Li, Na, K, Mg and Ca atoms, respectively.

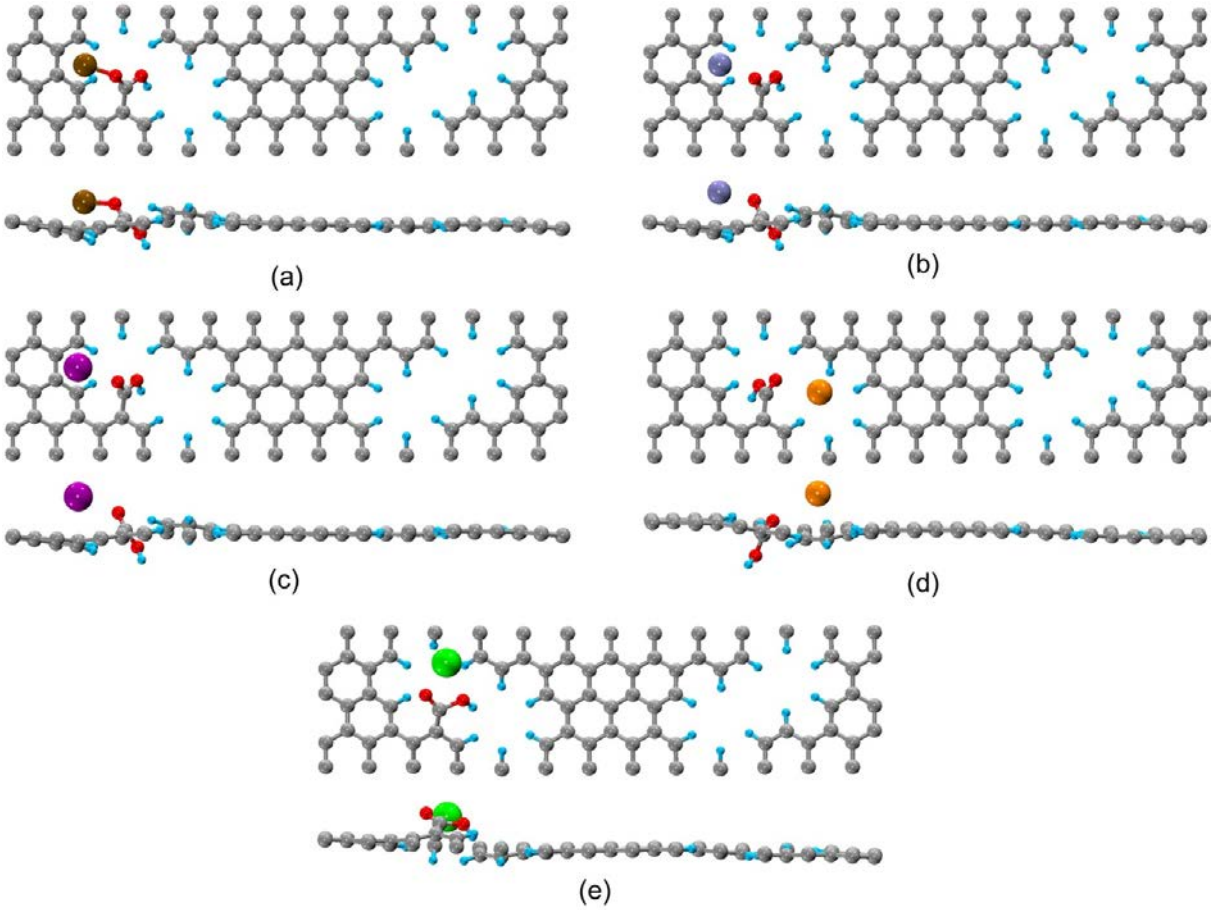

Figure 5: Top and side views of the optimized structures of (a) Li@COOH-NPG (b) Na@ COOH-NPG (c) K@ COOH-NPG (d) Mg@ COOH-NPG and (e) Ca@ COOH-NPG. Grey, blue, red, brown, purple, magenta, orange and green balls represent C, H, O, Li, Na, K, Mg and Ca atoms, respectively.

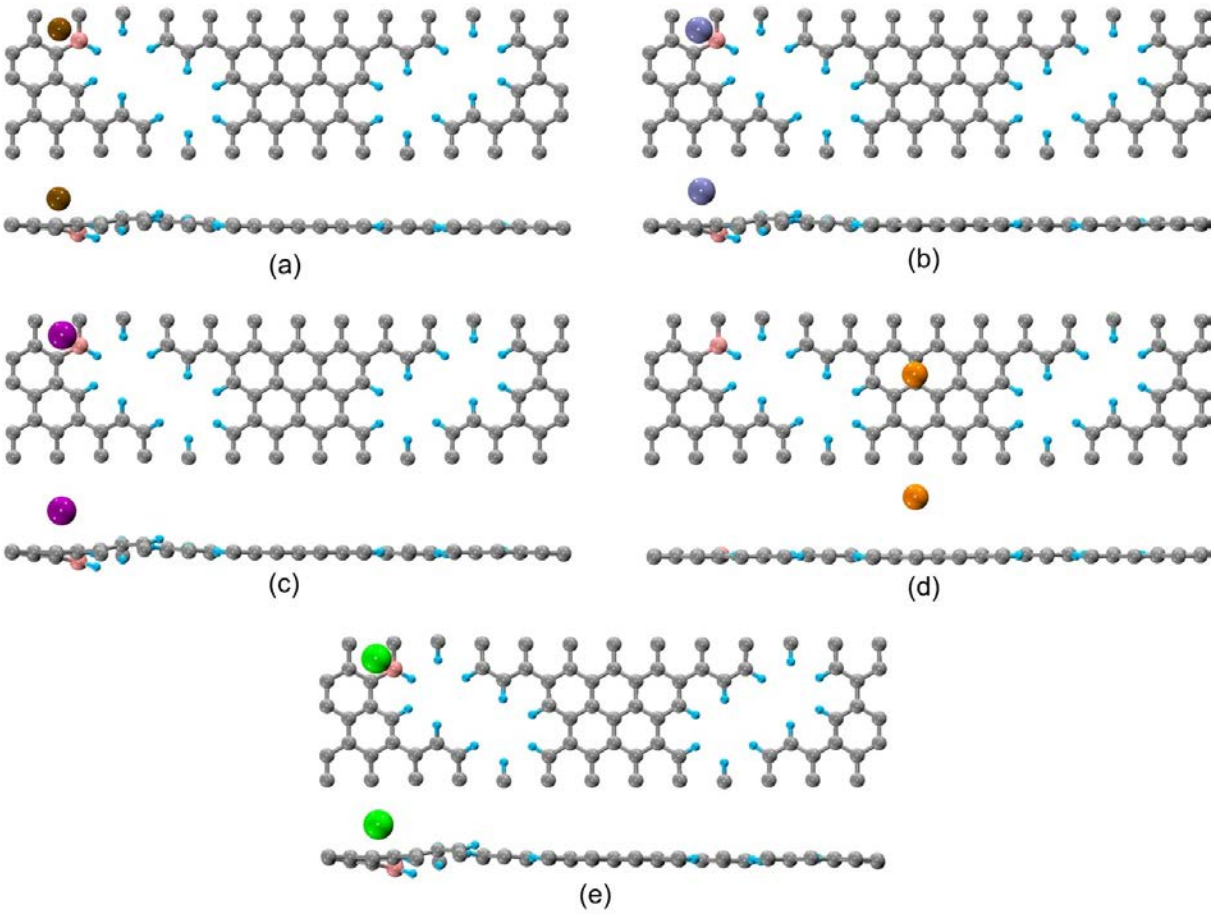

Figure 6: Top and side views of the optimized structures of (a) Li@B-NPG (b) Na@B-NPG (c) K@B-NPG (d) Mg@B-NPG and (e) Ca@ B-NPG. Grey, blue, orange, brown, purple, magenta, dark orange and green balls represent C, H, B, Li, Na, K, Mg and Ca atoms, respectively.

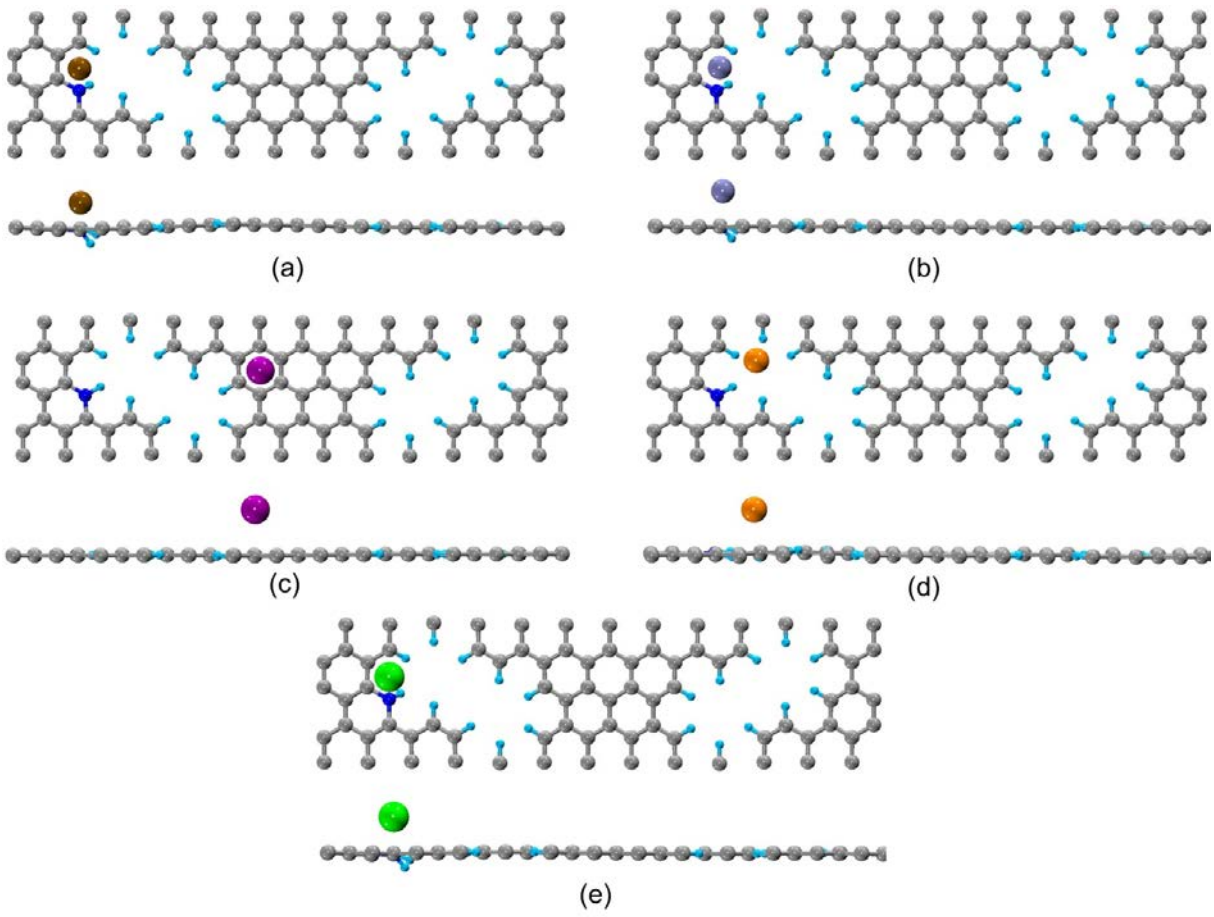

Figure 7: Top and side views of the optimized structures of (a) Li@N-NPG (b) Na@N-NPG (c) K@N-NPG (d) Mg@N-NPG and (e) Ca@ N-NPG. Grey, blue, dark blue, brown, purple, magenta, dark orange and green balls represent C, H, N, Li, Na, K, Mg and Ca atoms, respectively.

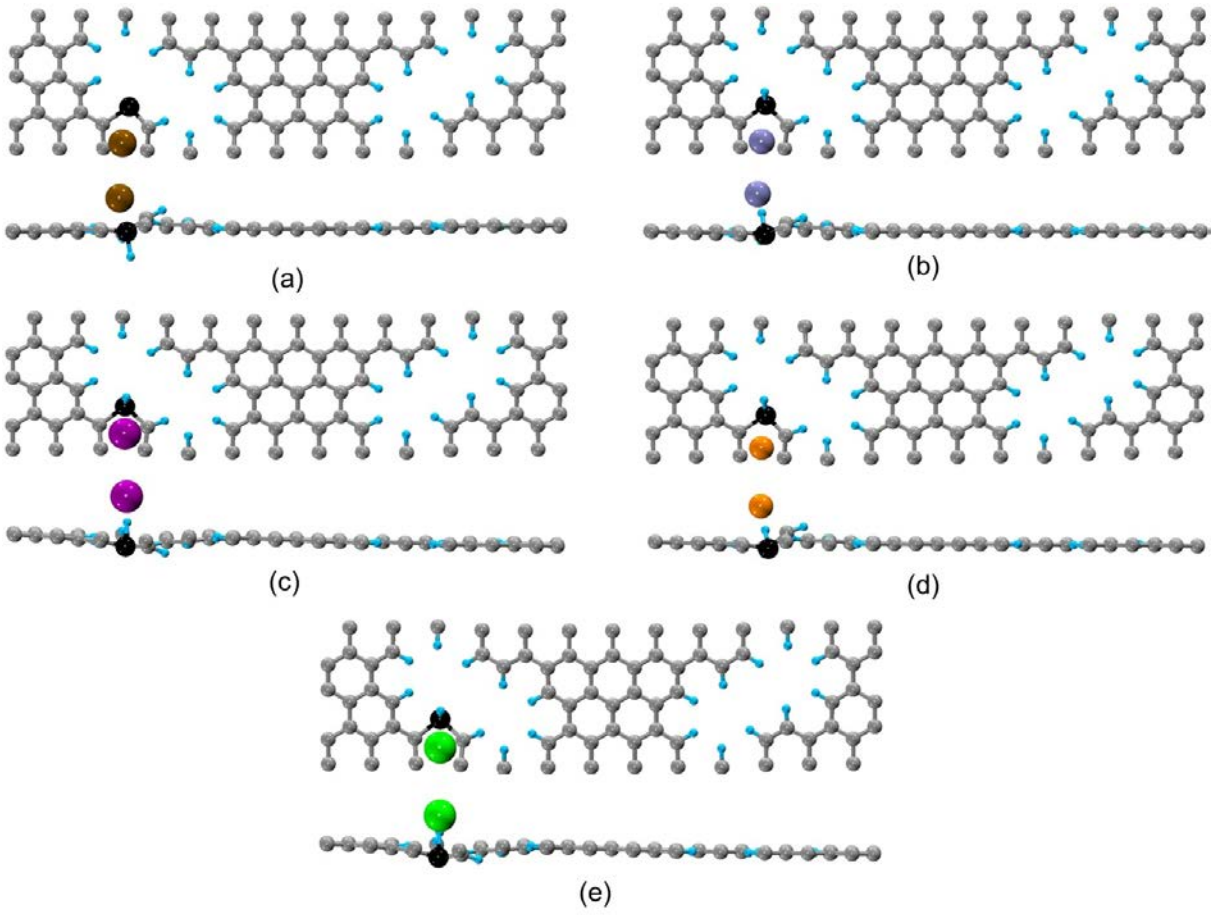

Figure 8: Top and side views of the optimized structures of (a) Li@P-NPG (b) Na@P-NPG (c) K@P-NPG (d) Mg@P-NPG and (e) Ca@ P-NPG. Grey, blue, black, brown, purple, magenta, dark orange and green balls represent C, H, P, Li, Na, K, Mg and Ca atoms, respectively.

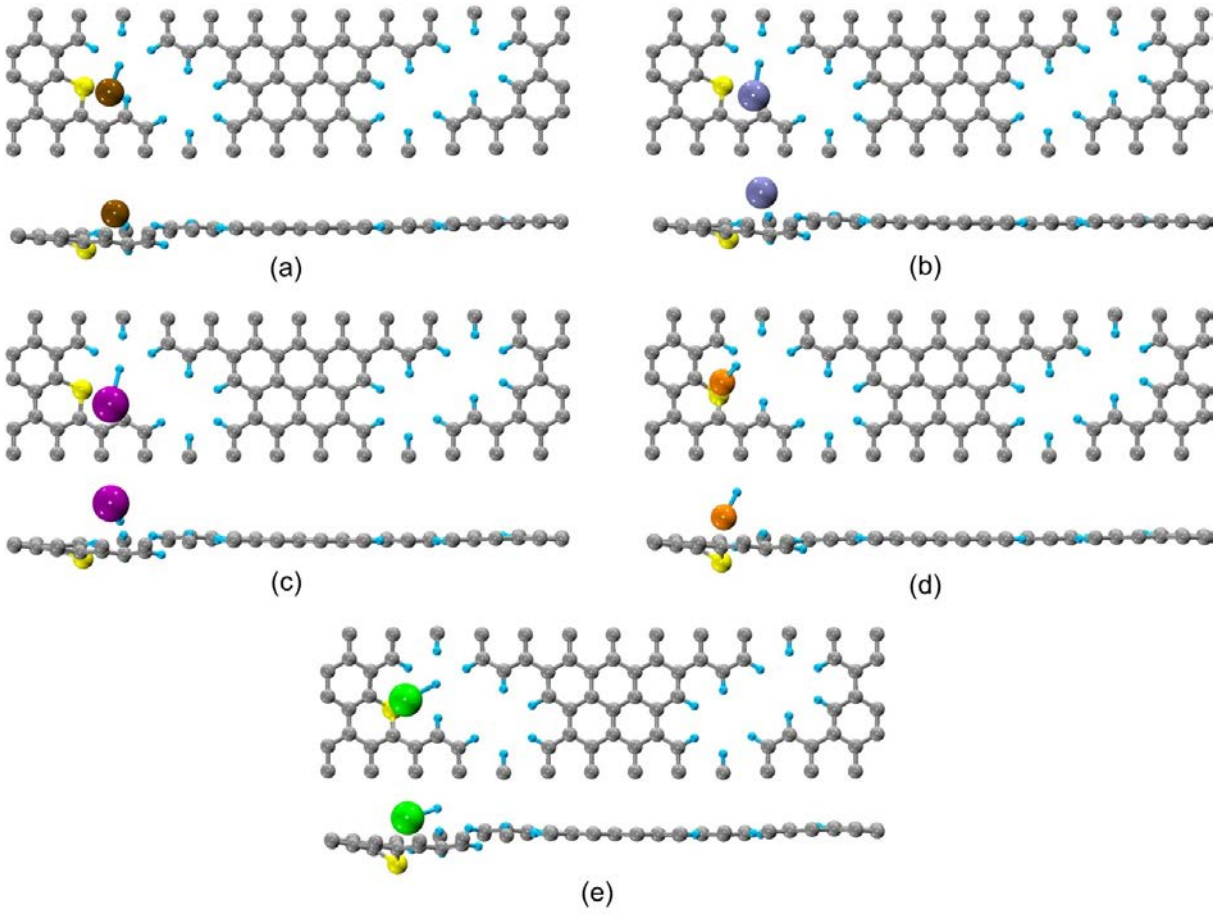

Figure 9: Top and side views of the optimized structures of (a) Li@S-NPG (b) Na@S-NPG (c) K@S-NPG (d) Mg@S-NPG and (e) Ca@ S-NPG. Grey, blue, yellow, brown, purple, magenta, dark orange and green balls represent C, H, S, Li, Na, K, Mg and Ca atoms, respectively.